Acta Crystallographica Section D
Biological Crystallography
ISSN 0907-4449

Structure of monkey dimeric dihydrodiol dehydrogenase in complex with isoascorbic acid

Vincenzo Carbone,[a] Rie Sumii,[b] Shuhei Ishikura,[b] Yukuhiko Asada,[b] Akira Hara[b] and Ossama El-Kabbani[a]*

[a]Department of Medicinal Chemistry, Victorian College of Pharmacy, Monash University, Parkville, Victoria 3052, Australia, and [b]Laboratory of Biochemistry, Gifu Pharmaceutical University, Mitahora-higashi, Gifu 502-8585, Japan

Correspondence e-mail: ossama.el-kabbani@vcp.monash.edu.au

Received 24 December 2007
Accepted 15 February 2008

PDB Reference: dihydrodiol dehydrogenase–isoascorbic acid complex, 2poq, r2poqsf.

Mammalian dimeric dihydrodiol dehydrogenase (DD) is identical to NADP$^+$-dependent D-xylose dehydrogenase. A recent investigation showed that the three-dimensional structure of monkey DD is similar to those of prokaryotic NADP(H)-dependent glucose-fructose oxidoreductase (GFO) and 1,5-anhydro-D-fructose reductase (AFR); however, it differs in coenzyme-binding and catalytic residues. Dimeric DD has a high affinity for NADP(H) when compared with AFR and differs from both GFO and AFR in its specificity for sugars and hydrophobic xenobiotic compounds as substrates. The crystal structure of monkey dimeric DD complexed with the inhibitor isoascorbic acid has been determined at 2.59 Å resolution. Molecular modelling of coenzyme binding complemented with site-directed mutagenesis has been utilized to propose a binding mode for the coenzyme molecule and to gain insights into the roles of the residues comprising the active site and coenzyme-binding domain of DD. Several key residues have been identified within the coenzyme-binding domain, including Arg37, Arg41, His76 and His79, that contribute to the high affinity for coenzyme. The interaction of Arg37 and Arg41 with the 2′-phosphate and adenine-ring moiety of the coenzyme has been established from the large increases (29-fold to 438-fold) in the K_d values for NADP(H) for the R37D and R41D mutant enzymes. The mutation of several residues lining the inhibitor-binding site of DD suggested the involvement of Trp125, Phe154, Trp254 and Phe279 in determining the broad substrate specificity and inhibitor potency of the enzyme. In addition, mutants of Lys97, which is present near the catalytic residue Tyr180, greatly reduced the k_{cat} value without changing the K_d values for coenzyme, suggesting the importance of Lys97 in the catalytic mechanism of DD.

1. Introduction

Dihydrodiol dehydrogenase (DD; EC 1.3.1.20) catalyzes the NADP$^+$-linked oxidation of dihydrodiols of aromatic hydrocarbons to their corresponding catechols and has been regarded as a toxication enzyme in the metabolism of carcinogenic polycyclic aromatic hydrocarbons because oxidation by the enzyme yields reactive and redox-active *o*-quinones and reactive oxygen species (Penning, 2004). In mammalian tissues DD exists in several multiple forms, which are divided into two groups: monomeric and dimeric enzymes. Most monomeric forms of the enzyme have been shown to be identical to enzymes in the aldo-keto reductase (AKR) superfamily (Hyndman *et al.*, 2003), such as aldehyde reductase and some hydroxysteroid dehydrogenases (Penning, 2004; Wörner & Oesch, 1984; Hara, Nakayama *et al.*, 1991; Hara et

al., 1996; Deyashiki *et al.*, 1995), whereas dimeric DD, which is composed of 36 kDa subunits, shows a substrate specificity and a primary structure that are distinct from those of the monomeric DDs. Dimeric DD oxidizes several pentoses and some hexoses and has been identified as an $NADP^+$-dependent D-xylose dehydrogenase (EC 1.1.1.179; Aoki *et al.*, 2001; Zepeda *et al.*, 1990). The enzyme also reduces reactive carbonyl compounds such as methylglyoxal and 3-deoxyglucosone, as well as several hydrophilic carbonyl compounds such as camphorquinone (CQ) and nitrobenzaldehydes (Nakagawa *et al.*, 1989; Nakayama *et al.*, 1990; Sato *et al.*, 1994). This broad substrate specificity indicates additional roles of the enzyme in the metabolism of endogenous and xenobiotic carbonyl compounds and the prevention of the development of glycation. Mammalian dimeric DDs have a high degree of interspecies sequence similarity (>82%; Arimitsu *et al.*, 1999), but show no homology to enzymes belonging to the AKR and short-chain dehydrogenase/reductase (SDR) superfamilies (Oppermann *et al.*, 2003). Dimeric DD shows low sequence similarity (17–41% identity) to 20 putative gene products from microorganisms and to *Zymomonas mobilis* glucose-fructose oxidoreductase (GFO; EC 1.1.99.28) and it has been proposed that these proteins constitute a family of enzymes with two consensus sequences, His-X_{16}-Glu-Lys-Pro and Gly-X_3-Asp-*X*-Gly-*X*-Tyr (Arimitsu *et al.*, 1999). A previous mutagenesis study of monkey dimeric DD suggested that His79 in the former sequence functions in coenzyme binding and that Tyr180 in the latter sequence is critical for the reaction mechanism (Asada *et al.*, 2000).

A recent crystallographic study of monkey dimeric DD (Carbone *et al.*, 2008) has shown that the N-terminal half of the enzyme sequence forms a classical dinucleotide-binding domain consisting of two $\beta\alpha\beta\alpha\beta$ motifs and that the C-terminal sequence constitutes an eight-stranded predominantly antiparallel β-sheet. The C-terminal domain contains the active site of the enzyme and is also involved in the intermolecular contacts between monomers (*via* their respective β-sheets) that help to stabilize the quaternary structure. Confirming the previous sequence analysis of dimeric DD (Arimitsu *et al.*, 1999), no structural correlations with enzymes of the AKR and SDR superfamilies was observed. However, evaluation of the secondary-structure elements revealed a striking resemblance to several bacterial oxidoreductases, including *Z. mobilis* GFO (Nurizzo *et al.*, 2001; Kingston *et al.*, 1996) and *Sinorhizobium morelense* 1,5-anhydro-D-fructose reductase (AFR; Dambe *et al.*, 2006). GFO and dimeric DD are similar with respect to the catalytic residues (Tyr217 and Tyr180, respectively), but it remains unknown whether their catalytic mechanisms are identical. In addition, dimeric DD differs from the sugar-specific GFO and AFR in its broad substrate specificity for both sugars and hydrophobic xenobiotic compounds.

Here, we report the crystal structure of monkey dimeric DD in complex with the inhibitor isoascorbic acid (IA; Hara, Shinoda *et al.*, 1991). In an effort to further characterize the inhibitor-binding site, we have compared and contrasted the active-site interactions of IA with the recently solved structure of DD complexed with the inhibitor 4-hydroxyacetophenone (4OH; Carbone *et al.*, 2008; Shinoda *et al.*, 1992). Molecular-modelling studies involving secondary-structure matching of NADPH-dependent enzymes coupled with energy minimization have also made it possible to identify the roles of several key residues in coenzyme binding. These results, complemented with site-directed mutagenesis, kinetic and binding studies, suggest possible roles for several residues in the catalytic function of enzymes belonging to the same protein family in general and of dimeric DD in particular.

2. Materials and methods

2.1. Materials

Coenzymes and chemicals of the highest purity were purchased from Sigma–Aldrich Chemical Co., Fluka and Merck. Crystallization buffers and kits were purchased from Hampton Research.

2.2. Site-directed mutagenesis, expression and purification

Mutagenesis was performed using a QuikChange site-directed mutagenesis kit (Stratagene) and an expression pRset vector harbouring the cDNA for monkey DD14. The mutagenic primers were designed to produce the mutant DD enzymes (A36D, R37A, R37D, R41A, R41D, H76Q, H79Q, K97M, K97R, W125Y, W254Y, W254A, F154A, F279A and D280A) by replacing the respective codons in the cDNA sequence. The complete coding regions of the cDNAs were sequenced using a CEQ2000XL DNA sequencer (Beckman Coulter) to confirm the presence of the desired mutations and to ensure that no other mutations had occurred. The wild-type protein and those encoded by the mutated cDNAs were expressed in *Escherichia coli* BL21 (DE3) and the recombinant enzymes were purified from the 12 000*g* supernatants of the homogenates of the cells (500 ml cultures) as described previously (Arimitsu *et al.*, 1999; Asada *et al.*, 2000). The protein concentration was determined by the method of Bradford (1976) using bovine serum albumin as a standard.

2.3. Enzyme assay

The dehydrogenase and reductase activities of the enzyme were assayed by measuring the rate of change of NADP(H) fluorescence (at 455 nm with an excitation wavelength of 340 nm) and its absorbance (at 340 nm), respectively (Asada *et al.*, 2000). The standard reaction mixture for the dehydrogenase-activity assay consisted of 25 m*M* Tris–HCl pH 7.5, 0.25 m*M* $NADP^+$, 50 m*M* D-xylose and enzyme in a total volume of 2.0 ml. The reductase activity was determined using 0.1 m*M* NADPH and CQ as the coenzyme and the substrate, respectively. One unit (U) of activity was defined as the amount of enzyme that catalysed the formation of 1 µmol NADPH per minute at 298 K. The apparent K_m and k_{cat} values were determined using five concentrations of substrate or coenzyme in the presence of saturated concentrations of the corresponding coenzyme or substrate by fitting the initial velocities to the Michaelis–Menten equation. IC_{50} (the

Table 1
Data-collection and refinement statistics.

Values in parentheses are for the highest resolution shell.

Data-collection statistics	
Wavelength (Å)	1.54178
Resolution range (Å)	20–2.59 (2.68–2.59)
No. of observed reflections	116802
No. of unique reflections	17128
$R_{merge}(I)$ (%)	6.6 (25.7)
Completeness (%)	99.8 (98.0)
Redundancy	6.8
$I/\sigma(I)$	16.5 (4.9)
Refinement statistics	
Resolution range (Å)	19.9–2.59
No. of reflections used	17128
Size of R_{free} set (%)	5
R_{cryst}/R_{free} (%)	17.0/23.4
R.m.s.d.	
Bonds (Å)	0.022
Angles (°)	2.11
Ramachandran plot	
Residues in most favoured regions (%)	91.3
Residues in additional allowed regions (%)	8.4
Residues in disallowed regions (%)	0.3
Estimated coordinate error	
Luzzati mean error† (Å)	0.267
Mean B factor (Å^2)	
Protein	26.5
Isoascorbic acid	59.8
Sulfate	58.1
β-Mercaptoethanol	22.5
Water	30.0

† Luzzati (1952).

concentration required for 50% inhibition) values for IA and 4OH were determined in the CQ reduction because the inhibitors are uncompetitive with respect to CQ (Hara, Shinoda *et al.*, 1991; Shinoda *et al.*, 1992). The kinetic constants are expressed as the means of at least three determinations in which all standard errors were less than 20%.

2.4. Fluorescence

A fluorescence emission spectrum of the enzyme (2 µ*M*) was measured in 10 m*M* potassium phosphate pH 7.4 containing 20% glycerol at an excitation wavelength of 295 nm at 298 K using a Hitachi F-2000 spectrofluorometer. The fluorescence was quenched by the addition of NADP(H) and the dissociation constants (K_d) for the coenzymes were determined by measuring the intrinsic fluorescence of the protein as described previously (Asada *et al.*, 2000).

2.5. Crystallization

The inhibitor complex of monkey dimeric DD was crystallized using a solution consisting of 30 µl protein solution (24.7 mg ml^{-1} in 10 m*M* Tris–HCl pH 8.5 and 2 m*M* 2-mercaptoethanol at 277 K) mixed with 4 µl coenzyme solution (NADP$^+$; 42.8 m*M*) and 0.61 µl inhibitor solution (IA; 64.04 m*M*), which gives a 1:4:4 protein:coenzyme:inhibitor molar ratio and a final protein concentration of 23.4 mg ml^{-1} prior to crystallization. Each droplet consisted of 5 µl of the DD/NADP$^+$/IA solution mixed with 5 µl of a solution containing 2 *M* ammonium sulfate, 0.1 *M* sodium citrate buffer pH 5.0. Crystals were obtained at 293 K in a 24-well tissue-culture plate *via* the vapour-diffusion method (McPherson, 1985) and grew to average dimensions of 0.4 × 0.1 × 0.1 mm within 48 h.

2.6. X-ray data collection, processing and structural refinement

Diffraction data for the enzyme–inhibitor complex were collected at 100 K from crystals flash-cooled in cryoprotectant (2 *M* ammonium sulfate, 0.1 *M* sodium citrate buffer pH 5.0 and 25% glycerol) using a MAR345 detector mounted on a Rigaku RU-300 rotating-anode X-ray generator operated at 50 kV and 90 mA. Each frame was recorded with 1800 s exposure and 1.0° oscillation around φ. The crystal-to-detector distance was set to 250 mm. The data were processed and scaled using the *marHKL* software package (Otwinowski & Minor, 1997). A near-complete data set was collected to a maximum resolution of 2.59 Å in the hexagonal space group $P6_122$, with unit-cell parameters $a = b = 122.832$, $c = 121.293$ Å, $\alpha = \beta = 90.0$, $\gamma = 120.0°$. There was one monomer per asymmetric unit, with a solvent content estimated to occupy 66.01% of the unit-cell volume (Matthews, 1968) and a Matthews coefficient of 3.60 Å^3 Da^{-1}. Initial phases for the inhibitor complex were determined using the molecular-replacement program *MOLREP*, which is part of the *CCP*4 program suite (Collaborative Computational Project, Number 4, 1994), using data in the resolution range 19.99–3.0 Å and the high-resolution structure of DD (PDB code 2o4u; Carbone *et al.*, 2008) as a model. The initial model was subjected to structural refinement using *REFMAC* (Murshudov *et al.*, 1997). Difference Fourier maps ($2F_o - F_c$ and $F_o - F_c$) were visualized in *Coot* (Emsley & Cowtan, 2004) and enabled the addition of bound substituents and water molecules. Additional refinement, data-collection and processing statistics are shown in Table 1.

2.7. Molecular modelling

Since crystallographic analysis did not reveal electron density for bound coenzyme, proteins with similar coenzyme-binding domains were identified and used to construct a model of the DD ternary complex. The N-terminal portion of DD (residues 1–123; Carbone *et al.*, 2008) was subjected to analysis by the online secondary-structure matching tool *SSM* (Krissinel & Henrick, 2004) and coenzyme-binding domains with the lowest r.m.s.d. and best *Q*-score values were visualized using the molecular-graphics program *Coot* (Emsley & Cowtan, 2004). The crystal structure coordinates of GFO (PDB code 1ofg; Kingston *et al.*, 1996), AFR (PDB code 2glx; Dambe *et al.*, 2006), dihydrodipicolinate reductase (DPR; PDB code 1c3v; Cirilli *et al.*, 2003) and the predicted dehydrogenase/oxidoreductase TM0312 (TMO; PDB code 1zh8; Chhabra *et al.*, 2003) were used to construct models of the DD ternary complex (DD–NADP$^+$–IA). Taking into account the relative distance between residues and torsion angles, the rotamer conformations of clashing residues were changed to

Table 2
Results of superposition of the N-terminal domain (residues 2–125; Krissinel & Henrick, 2004) of DD on structurally related proteins.

Intermolecular binding energies between the coenzyme and protein following energy minimization are also reported.

Protein (PDB code)	R.m.s.d.† (Å)	*Z* score‡	ΔH (kJ mol^{-1})
1,5-Anhydro-D-fructose reductase (2glx)	1.40	10.1	−346.0
Glucose-fructose oxidoreductase (1ofg)	1.54	9.8	−456.0
Dihydrodipicolinate reductase (1c3v)	1.72	8.9	−346.7
Oxidoreductase (TM0312) (1zh8)	1.76	6.8	−487.1

† The root-mean-square deviation calculated between C^{α} atoms of matched residues of the query and target structures. ‡ A measure of the statistical significance of a match in terms of Gaussian statistics.

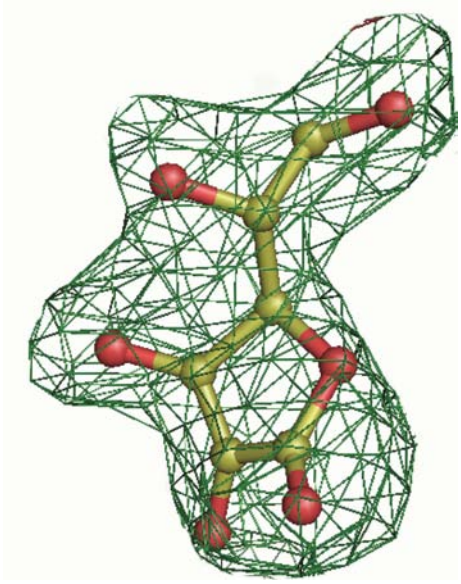

Figure 1
The final electron-density OMIT map ($F_o - F_c$) calculated at 2.59 Å resolution (2.5σ cutoff) for IA. This figure was prepared using *PyMOL* (DeLano, 2002).

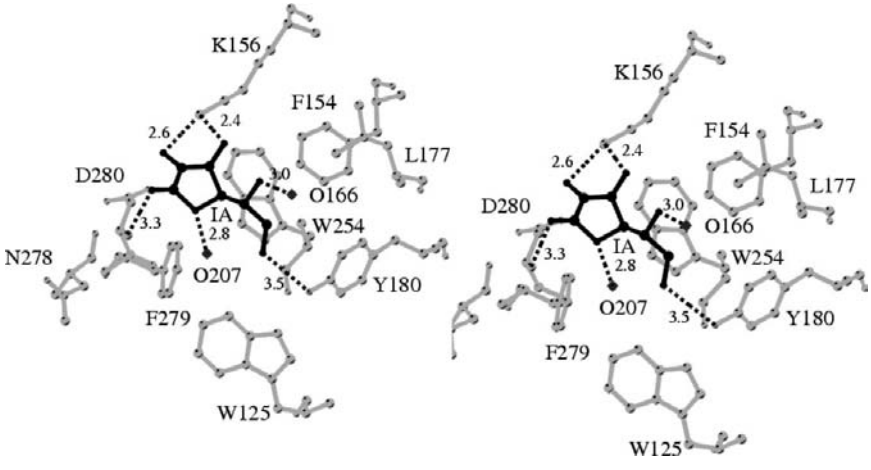

Figure 2
Stereoview of IA in the active site of DD. Residues within 4 Å of the inhibitor are shown. Hydrogen bonds to side chains and waters (O) are depicted as dashed lines and their distances are given in angstroms. This figure was prepared using *MolScript* (Kraulis, 1991).

fit the superimposed coenzyme where necessary in order to conserve the conformational aspects of the molecule.

To relieve any steric hindrance associated with the superimposed coenzyme, energy minimization was carried using the *Discover* 2.7 program (Biosym Technologies, San Diego, California, USA) on a Linux workstation following established procedures that had been found to be effective in examining conformational space for a protein–ligand complex (Darmanin & El-Kabbani, 2000, 2001). Calculations including a constant-valence force field incorporating the simple harmonic function for bond stretching and excluding all nondiagonal terms were carried out (cutoff distance of 26 Å) using the steepest-descent and conjugate-gradient algorithms (down to a maximum atomic root-mean-square derivative of 41.9 and 0.04 kJ Å^{-1}, respectively). Force-field potentials and partial charges were automatically assigned and visualized using *Insight*II, with the contributions of the proposed residues to the binding of $NADP^+$ calculated using *Discover*. Additionally, the crystal structures of DD containing IA and 4OH (PDB code 2o48) were used to extract the contribution of the active-site residues towards inhibitor binding.

3. Results

3.1. Crystallography

The crystal structure of DD in complex with IA was determined at 2.59 Å resolution, with final R_{cryst} and R_{free} values of 17.0% and 23.4%, respectively. Like the previous crystal structures of DD, the electron density was non-existent for the coenzyme and poor for the N-terminal methionine and the C-terminal residues Lys333 and His334. The asymmetric unit consisted of 331 amino acids, one IA molecule bound in the active site of the protein, 211 waters, four sulfate molecules and one 2-mercaptoethanol molecule covalently bound to Cys253. Stereochemical and geometric statistics for the final model are shown in Table 1.

3.2. The catalytic domain

The refinement of DD revealed continuous electron density for the inhibitor IA in the active site of the protein (Fig. 1). IA is a competitive inhibitor with respect to the dihydrodiols of benzene and napthalene (Hara, Shinoda *et al.*, 1991) and forms a number of important side-chain interactions with active-site residues (Fig. 2). These include interactions *via* the hydroxyl groups at C3 and C4 of the furanone ring of IA, which make hydrogen-bond contacts with the side-chain N atom (NZ) of Lys156 (2.4 and 2.6 Å, respectively), while the C2 hydroxyl of IA forms an additional hydrogen bond to the catalytic side-chain hydroxyl (OH) of Tyr180 (3.5 Å; Asada *et al.*, 2000). The carbonyl group on the furanone ring forms a hydrogen-bond interac-

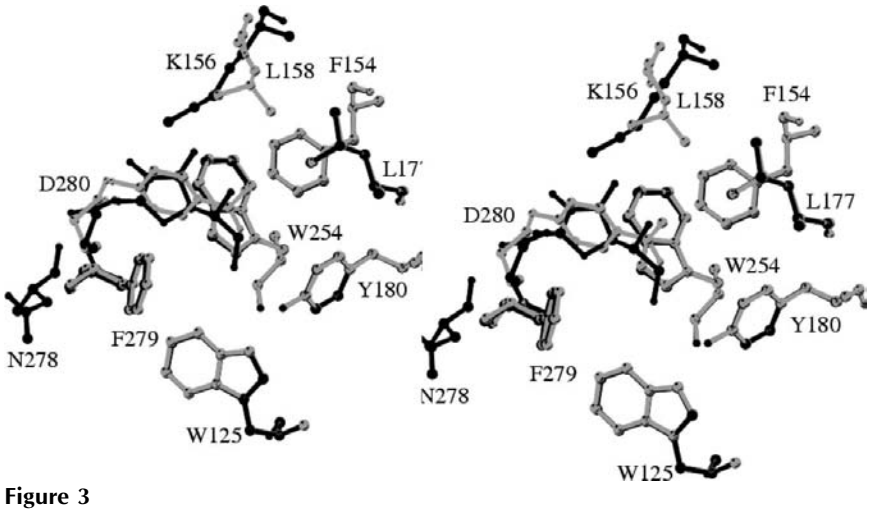

Figure 3
Superposition of the inhibitor-binding site residues of DD containing IA (black) and 4OH (grey). This figure was prepared using *MolScript* (Kraulis, 1991).

tion with the main-chain N atom of Asp280 (3.3 Å), while residues including Phe279, Asn278, Trp254, Leu177, Phe154 and Trp125 form a number of van der Waals and hydrophobic contacts with the inhibitor. Additionally, two water molecules (O207 and O166) fall within hydrogen-bonding distance of the oxygen species present on the furanone ring (O) and the C1 hydroxyl group of IA (2.8 and 3.0 Å, respectively). The likely presence of these and other water molecules in the predominantly hydrophobic active site of DD is in part a consequence of the absence of $NADP^+$; the waters interact with charged residues including Glu96 and Lys97 instead of the nicotinamide ring of the coenzyme.

To further identify the relative importance of active-site residues with regard to DD inhibition, the crystal structures containing IA and 4OH were superimposed and scrutinized (Fig. 3). 4OH has been identified as a potent inhibitor of DD (Shinoda *et al.*, 1992) and occupies a similar position in the active site compared with IA in the DD–IA complex. The C-terminal loop, which defines a large section of the active-site domain (Carbone *et al.*, 2008), was found not to undergo a conformational change when bound to either inhibitor. Such an observation is related to the molecular sizes of the compounds (see Fig. 4) rather than their inhibitory potencies; while 4OH is the smaller compound of the two, it is a more potent inhibitor of DD than IA (IC_{50} values of 0.97 and 38 μM, respectively). 4OH is not in direct contact with the catalytic residue Tyr180 and instead forms a close van der Waals interaction with the side-chain atoms of Asp280; this is noticeable by the change in rotamer conformation of the side chain between the two crystal structures. However, the most defining characteristic of the DD–4OH complex is the large number of hydrophobic contacts that 4OH forms with residues Phe279, Trp254 Leu158 and Leu177. IA forms similar contacts but fewer are hydrophobic in nature; often weak van der Waals interactions are formed between a hydrophobic residue and a hydrophilic functional group such as a carbonyl or hydroxyl. The affinity of the inhibitor for the protein was further examined *via* binding-energy calculations performed on the crystal structures of the DD complexes. The protein interaction energies measured for 4OH and IA in the active site of DD indicated a fivefold preference for 4OH over IA (−105.6 and −24.4 kJ mol^{-1}, respectively), which is consistent with the differences in their inhibitory constants (0.2 and 11 μM, respectively) measured in solution (Hara, Shinoda *et al.*, 1991; Shinoda *et al.*, 1992).

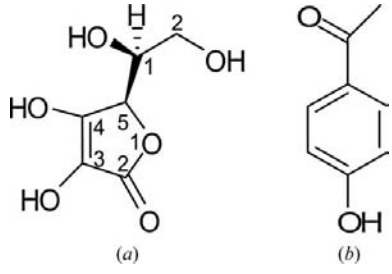

Figure 4
Chemical structures of the DD inhibitors IA {*R*-5-[(1*R*)-1,2-dihydroxyethyl]-3,4-dihydroxyfuran-2-one} (*a*) and 4OH (*b*).

3.3. Coenzyme-binding site

Like all previous crystal structures of DD solved to date, the DD–IA complex was solved with $NADP^+$ failing to bind to the enzyme during crystallization. In the area thought to contain the coenzyme molecule, two sulfate molecules form a number of hydrogen-bond contacts with residues including the main-chain N atoms of Val10 (3.1 Å), Leu12 (3.3 Å) and Arg37 (3.1 Å) and the side-chain atoms of Arg41 (NH1 and NE, 2.5 and 3.0 Å), Tyr58 (OH, 2.7 Å), Arg163 (NH1, 2.7 Å) and Gln75 (NE2; 3.0 Å). In order to obtain an understanding of the coenzyme-binding domain and the intermolecular hydrogen bonds formed with DD, we utilized the online secondary-structure matching tool *SSM* (Krissinel & Henrick, 2004) and molecular-modelling techniques to produce a ternary model of DD. Like previous results (Arimitsu *et al.*, 1999; Carbone *et al.*, 2008), little similarity was evident based on sequence alignment (<31% of N-terminal residues), with the majority of homologous structural candidates being bacterial oxidoreductases. Enzymes with bound $NADP^+$ were selected based on r.m.s.d. and *Z*-score values (summarized in Table 2), denoting exceptionally similar N-terminal architecture between DD and the candidate oxidoreductase. The enzymes selected included *Z. mobilis* GFO (Kingston *et al.*, 1996), *S. morelense* AFR (Dambe *et al.*, 2006), DPR from *Mycobacterium tuberculosis* (Cirilli *et al.*, 2003) and TMO with predicted dehydrogenase/oxidoreductase activity from *Thermotoga maritima* (Chhabra *et al.*, 2003). DD, TMO, AFR and GFO form similar structures displaying a Rossmann-fold element at the N-terminus and a C-terminus made up of a predominantly antiparallel β-sheet. DPR is the least homo-

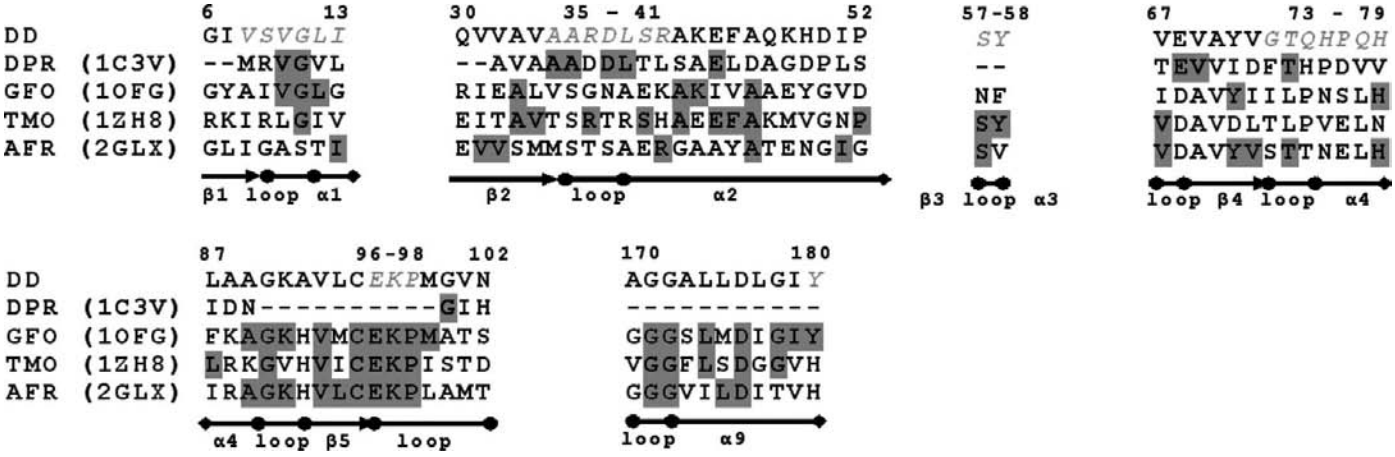

Figure 5
ClustalX (Thompson *et al.*, 1997) amino-acid sequence alignment of bacterial oxidoreductases with the portions of the N-terminal domain proposed to bind the coenzyme in mammalian DD. The enzymes are GFO from *Z. mobilis*, AFR from *S. morelense*, DPR from *M. tuberculosis* and TMO from *T. maritima*. The shaded regions indicate residue identity, with gaps denoted by dashes. PDB codes, residue numbers and secondary-structure elements such as loops, α-helices and β-sheets are indicated. The residues proposed to bind or interact with the coenzyme in DD are shown in italics.

logous, possessing a C-terminal domain containing four β-strands and two α-helices forming an open α,β-sandwich (Cirilli *et al.*, 2003). Sequence alignment of the candidate proteins using *ClustalX* (Thompson *et al.*, 1997) revealed several conserved residues/sequences between DD, TMO, AFR and GFO, but less conservation in DPR (Fig. 5). The coenzyme-binding site in DD, TMO, AFR and GFO is comprised of approximately 25 residues, including seven or eight residues that directly interact or form hydrogen bonds with the coenzyme. The most well known is the highly conserved Glu-Lys-Pro motif (residues 96–98), which has been identified in all mammalian DDs (Arimitsu *et al.*, 1999) and has been deduced to play a role in coenzyme binding and enzyme catalysis in GFO (Kingston *et al.*, 1996) and AFR (Dambe *et al.*, 2006).

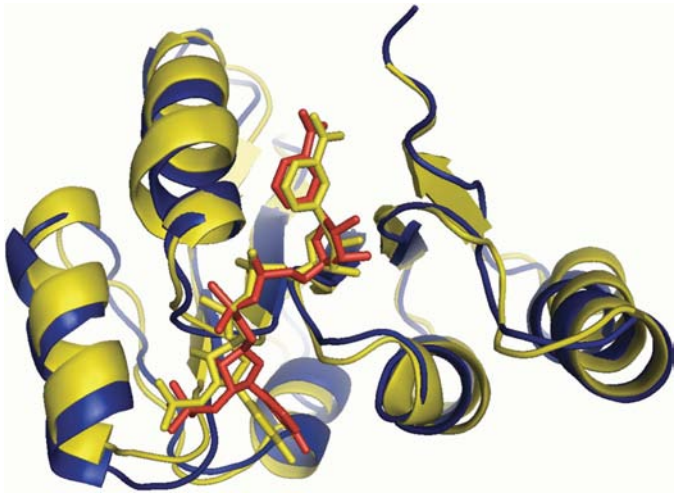

Figure 6
The superimposed N-terminal domains of DD (blue; residues 2–125) and the bacterial oxidoreductase from *T. maritima* (yellow; residues 4–129; PDB code 1zh8). DD and the NADP$^+$ molecule (red) modelled into the coenzyme-binding domain were produced following energy minimization. This figure was prepared using *PyMOL* (DeLano, 2002).

Prior to energy minimization, the coenzymes were assessed for any structural clashes with DD residues and alternate rotamer conformations were assigned, matching if possible the parent protein, assuming that similar interactions occur when NADP$^+$ is bound to DD. This most often included Lys97 and Tyr58, the side chains of which tended to point towards or into the nicotinamide and adenine rings, respectively, of NADP$^+$. The protein-interaction energies measured following energy minimization (Table 2) indicated that the conformations of NADP$^+$ found in TMO and GFO yielded the strongest binding energies when compared with those in AFR and DPR. Inspection of the models showed that of the four, NADP$^+$ from TMO underwent the smallest of changes prior to and following energy minimization (Fig. 6), suggesting a good fit and stereochemistry of the coenzyme in the coenzyme-binding pocket of DD, while NADP$^+$ from GFO produced the largest movements of the nicotinamide, 2′-ribose and adenine-ring moieties. This is understandable, as the stereochemistry of the coenzyme in GFO finds the nicotinamide ring in the *anti* conformation and the adenine ring in the *syn* conformation pointing above the ribose sugar (Kingston *et al.*, 1996). The adenine ring therefore fails to make any stabilizing or meaningful contacts; in the GFO tetramer interactions with N-terminal residues from an adjacent monomer are relied upon to firmly stabilize the nondissociable binding of the coenzyme. In the case of AFR (Dambe *et al.*, 2006), the adenine ring is in the *anti* position around the glycosidic bond (Fig. 7*a*) and its conformation is stabilized by stacking against the guanidinium group of Arg38. In the DD model, Arg41, which occupies the same position, does not form a similar interaction, further exacerbating the propensity for the adenine ring to point away from the coenzyme-binding pocket following energy minimization. In this case, the adenine ring is free of any side-chain residue interaction, as reflected by the lower energy score (Table 2). The molecular model was

therefore based on the minimized structure containing NADP$^+$ from TMO, which like NADP$^+$ from DPR has the nicotinamide and adenine rings in the classical *anti* conformation (Fig. 7*b*). The difference in coenzyme affinity between the two was attributed to a smaller number of meaningful interactions between a number of residues such as Arg37 and Arg41 and the pyrophosphate moiety of NADP$^+$.

The major interactions formed by the coenzyme of TMO included those with residues Val8, Ser9, Val10, Gly11, Leu12, Ile13, Ala35, Ala36, Arg37, Arg41, Gly73, Thr74, Gln75, His76, His79, Glu96, Lys97, Arg163 and Tyr180 (shown in the DD monomer in Fig. 8). The hydrogen bonds to DD are summarized in Fig. 9; however, a number of other important features are evident. The adenine ring and 2-ribose sugar are stabilized in part by the van der Waals interactions generated by the main-chain and side-chain residues of Val8, Ser9, Val10, Ala35, Ala36 and Tyr58 and in part by close stacking interactions with the side chain of Arg37 (3.5 Å). The short loops formed between the first and fourth β-strands and α-helices (βa and α1, βd and α4) help to maintain the orientation of the coenzyme by forming a series of rolling van der Waals interactions between the N atoms and carbonyls of the main chain with the pyrophosphate bridge and ribose sugars of NADP$^+$. The catalytic residue Tyr180, as well as Glu96, which is part of the Glu-Lys-Pro structural motif present in the loop between β-sheet 5 and α-helix 5, form hydrogen bonds and van der Waals interactions with the nicotinamide ring of NADP$^+$, while the hydroxyl groups on the ribose sugar form hydrogen-bond contacts with His76 and His79. The highly charged pyrophosphate moiety of NADP$^+$ forms multiple and exclusive hydrogen-bond contacts with the side-chain and main-chain N atoms of Arg37 and Arg41, as reflected by the relatively strong residue–coenzyme interaction energies of -72.8 and -28.5 kJ mol^{-1}, respectively.

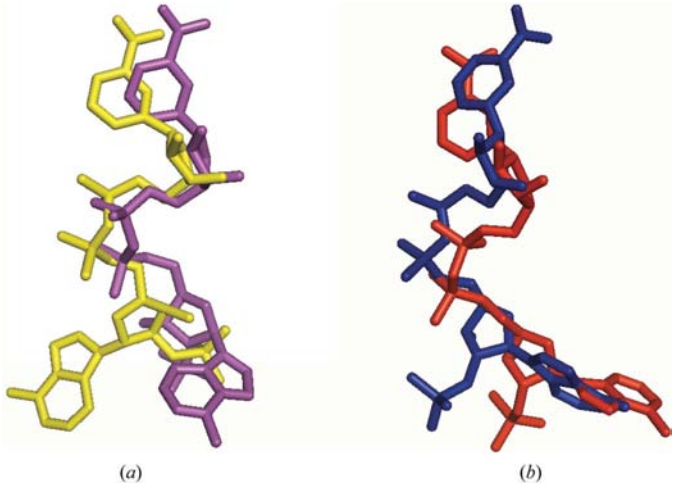

Figure 7
The superimposed coenzyme molecules (NADP$^+$) of (*a*) GFO (purple) and AFR (yellow) and (*b*) TMO (red) and DPR (blue) following minimization within the coenzyme-binding pocket of DD. The *syn* conformation of the adenine ring in GFO and the *anti* conformation around the glycosidic bond in AFR relay large differences in stereochemistry for the coenzymes. Both DPR and TMO have the same *anti* conformation of the nicotinamide and adenine ring, with the orientation of the pyrophosphate moiety accounting for the large changes in coenzyme-binding affinity. This figure was prepared using *PyMOL* (DeLano, 2002).

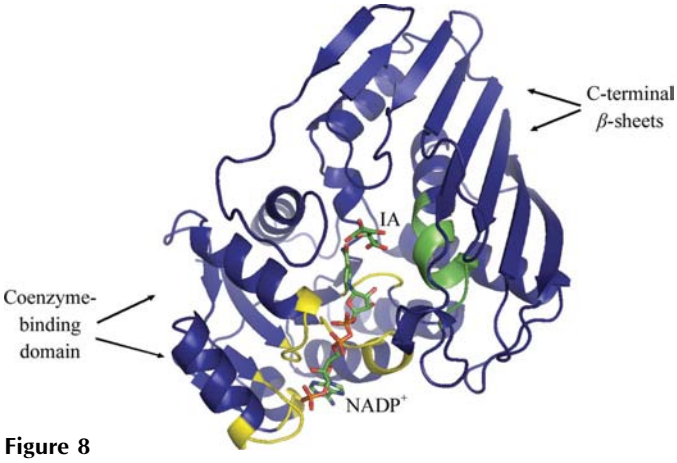

Figure 8
The monomer of DD presented in ribbon form. IA and the modelled NADP$^+$ are also presented, with the active-site helix containing the consensus sequence shown in green and residues interacting with the coenzyme shown in yellow. This figure was prepared using *PyMOL* (DeLano, 2002).

3.4. Site-directed mutagenesis

Dissociation constants for NADP(H) are summarized in Table 3 for a selection of mutated candidate coenzyme-binding residues. With the exceptions of K97M and K97R, the mutant enzymes showed higher K_d values for coenzyme than the wild-type enzyme (WT). The greatest effect was observed by the replacement of Ala36 by Asp, followed by the replacement of Arg37 and Arg41 by Asp. While the replacement of Arg37 and Arg41 by Ala had a smaller effect on the binding of coenzyme in comparison to replacement by Asp, the effect is larger than that caused by a H79Q mutation

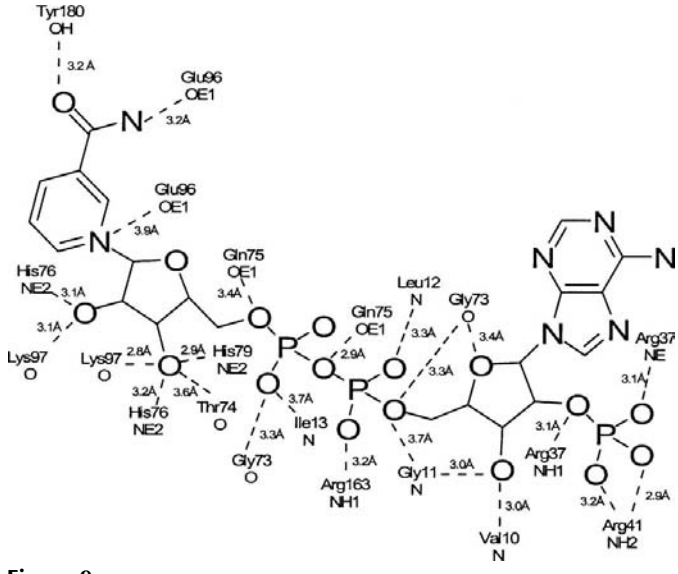

Figure 9
The hydrogen-bonding interactions and distances (Å) between the modelled NADP$^+$ molecule and amino-acid residues of the coenzyme-binding pocket.

Table 3
Alteration of K_d for coenzymes by the mutation of proposed putative coenzyme-binding residues.

		Mutant enzyme/WT ratio†								
	WT	K97M	K97R	H76Q	H79Q‡	A36D	R37A	R37D	R41A	R41D
Oxidation										
K_d NADP$^+$	0.18 μ*M*	0.4	0.6	5	7	>550§	16	94	14	29
K_m D-xylose	4.4 m*M*	nd	nd	41	15	65	3.4	11	2.3	2.9
k_{cat}	2.6 s^{-1}	na	na	0.5	0.9	0.45	1.2	0.4	1.7	1.0
Reduction										
K_d NADPH	0.13 μ*M*	1.6	0.5	8	8	784	92	438	20	108
K_m CQ	0.10 m*M*	11	17	21	5.1	12*	8.1	5.2*	3.1	2.4
k_{cat}	20 s^{-1}	0.004	0.004	3.6	0.6	0.02	2.1	0.05	1.2	0.9

† Kinetic constants were determined with saturated concentrations of the coenzymes (>14-fold increase in K_d) or substrates (greater than fivefold increase in K_m), except that 0.2 m*M* NADPH was used to estimate the K_m values for CQ where marked with an asterisk. ‡ Results previously published by Asada *et al.* (2000). § The enzyme was not saturated at 100 μ*M* NADP$^+$.

Table 4
Alteration of kinetic constants in oxidation and reduction and inhibitor sensitivity by mutagenesis of putative substrate-binding residues.

	D-Xylose oxidation†				CQ reduction†				Inhibitor sensitivity‡			
	K_m		k_{cat}/K_m		K_m		k_{cat}/K_m		IC_{50} for IA		IC_{50} for 4OH	
	(m*M*)	Ratio§	(s^{-1} m*M*$^{-1}$)	Ratio§	(m*M*)	Ratio§	(s^{-1} m*M*$^{-1}$)	Ratio§	(μ*M*)	Ratio§	(μ*M*)	Ratio§
W125Y	67	15	0.003	0.004	13	130	0.09	0.0005	4176	110	136	140
F154A	36	8	0.07	0.09	1.5	15	25	0.1	288	8	78	80
W254Y	14	3	0.29	0.4	0.84	8	40	0.2	38	1	6.0	6
W254A	90	20	0.02	0.03	3.6	36	6.1	0.03	66	2	83	86
F279A	89	20	0.02	0.03	26	260	0.6	0.003	3940	104	75	77

† Kinetic constants were determined with saturated concentrations (greater then fivefold increase in the respective K_m values) of the coenzymes. ‡ The IC_{50} values for IA and 4OH of WT were 38 and 0.97 μ*M*, respectively. The values for the mutant enzymes

(Asada *et al.*, 2000). The replacement of Ala36, Arg37 and Arg41 by a negatively charged residue resulted in >29-fold increases in the K_d value for NADP$^+$ with little change in the k_{cat} value. Collectively, these results indicate critical roles for both Arg37 and Arg41, particularly in the binding of NADP$^+$. This is supported by their electrostatic interactions with the negatively charged 2′-phosphate moiety of the docked NADP$^+$, while the formation of a hydrophobic pocket in part by Ala36 seems to be even more critical.

Compared with the large effects resulting from the mutation of Ala36, Arg37 and Arg41, the changes in the K_d values for coenzyme caused by the H76Q mutation were smaller (greater than a fivefold increase in K_d for NADPH and NADP$^+$), but were similar to those resulting from a H79Q mutation (Asada *et al.*, 2000). This observation supports the proximity of His76 and His79 to the ribose sugar in our model. His76 is not conserved in GFO and AFR; therefore, in addition to the above electrostatic bonds with the two Arg residues, the hydrogen-bond interaction between His76 and the coenzyme would account for the much lower K_m value in DD compared with that in AFR. Additionally, while His79 is buried behind the ribose sugar of NADP$^+$, His76 presents an open face towards the ribose of NADP$^+$ and the active site of DD. Its contribution to substrate binding may be minimal, although plausible, since it is present within 3.5 Å of the active-site residue Asp176 and its mutation causes a greater (>21-fold) increase in the K_m for substrate; this is twice the value resulting from the His79 mutation. The apparent lack of an effect resulting from the mutations K97M and K97R on the K_d values for coenzyme is also in agreement with the interactions of their main-chain carbonyl with the nicotinamide-ribose moiety of the coenzyme in our model. The replacement of the side chain does not affect coenzyme binding, whereas the mutation resulted in a drastic decrease in the catalytic activity of the enzyme.

Post energy minimization, IA does not radically change its conformation, maintaining its association with the active-site residues described in the crystal structure. The C2 hydroxyl of IA is present at a distance of 3 Å from the C4 C atom of the coenzyme and its distance to the side-chain hydroxyl (OH) of Tyr180 is 3.4 Å. This, together with the loss of enzymatic activity in the Y180F mutation (Asada *et al.*, 2000), suggests that Tyr180 is the proton donor/acceptor during catalysis, as few residues immediately adjacent to the modelled NADP$^+$ are capable of both or either duties. The side-chain N atom (NZ) of Lys97, part of the well preserved Glu-Lys-Pro motif, is within 3.2 Å of the side-chain hydroxyl (OH) of Tyr180 and partially stacks against the nicotinamide ring of NADP$^+$, as seen in the crystal structures of preGFOR–glucose (Nurizzo *et al.*, 2001). This residue was exceptionally sensitive to mutagenesis; the K97M and K97R mutants showed a total loss of activity for the oxidation reaction of DD and very low CQ reductase activity was observed (Table 3). Overall, our mutagenesis results suggest a similar positioning of the nicotinamide ring within the active site of the modelled ternary complex.

Mutation of the residues that form the substrate-binding cleft produced interesting results (Table 4). The mutation of predominantly large aromatic residues to smaller phenyl or methyl residues consistently increased the IC_{50} values for 4OH over IA, with the exception being Phe279, and in all cases increased the K_m values for CQ over D-xylose. The mutation of W254A, which resulted in the loss of an indole ring, produced larger changes in the K_m values for the substrates and IC_{50} values than the mutation W254Y. However, the changes are smaller than those displayed by the W125Y mutant, suggesting a greater importance of Trp125 (which is located at 3.6 Å from the modelled nicotinamide of the coenzyme) in the binding of substrate and inhibitor. We would suggest that while IA makes a hydrogen-bond interaction with Tyr180, the introduction of a hydroxyl group in the W125Y

mutant adjacent to the catalytic residue distorts or disrupts this interaction, affecting inhibitor potency. In the case of 4OH, the inhibitor makes an interaction with Tyr180 *via* a water molecule and its binding is likely to be affected in a similar manner by the mutation (Table 4). The mutation of Phe279, which is present on a loop region at the mouth of the active site (residues 268–281), to an alanine removes the close van der Waals and hydrophobic interactions that it forms with the inhibitors 4OH and IA, creating an overall increase in IC_{50} values (Table 4). Moreover, it is likely that the conformation of this loop region is influenced by the loss of the large hydrophobic side chain, affecting the interaction between the inhibitors and the main-chain imino group of Asp280 and resulting in the deviations observed in the IC_{50} values of IA and 4OH. In contrast, the D280A mutation did not have an effect on the binding of substrate and inhibitor (data not shown), confirming the contribution of the main-chain imino to inhibitor binding. The mutation F154A had a small effect on the IC_{50} value for IA, but resulted in a large change in the IC_{50} value for 4OH; this is comparable to the changes caused by the W254A mutation (Table 4). The side chains of Phe154 and Trp254 form a partial stacking interaction (3.5 Å) within a predominantly hydrophobic portion of the active site of DD that is removed by the F154A and W254A mutations. The W254Y mutation produced no change in the IC_{50} value for IA and mildly affected the potency of 4OH. This result suggests the importance of maintaining the stacking interaction between Phe154 and Trp254 in the binding of 4OH, unlike the binding of IA, in which hydrogen-bonding interactions play a greater role. It should be noted that the alteration of the K_m values for NADP(H) by these five mutations were less than threefold compared with the values for the WT.

4. Discussion

4.1. Implications for coenzyme binding

The crystal structure of the DD–IA complex has been solved and site-directed mutagenesis and molecular modelling were used to identify the residues critical for the binding of coenzyme and inhibitor. A common feature of the DD crystallization protocol is the formation of large robust crystals in buffers containing high phosphate or sulfate concentrations (>1.5 *M*; Carbone *et al.*, 2008), which are invariably bound in the refined crystal structure, consistently binding in a shallow pocket adjacent to the active-site domain of the protein where molecular modelling studies suggest that the coenzyme is bound. Steady-state kinetics experiments have shown a demonstrable decrease in affinity (K_m) for substrate and coenzyme or depressed DD activity to arise from increases in the concentration of salts such as phosphate and sulfate of usually equal to or less than 0.1 *M* in the reaction volume (Deyashiki *et al.*, 1995; Asada *et al.*, 2000; Sato *et al.*, 1993). Therefore, these salts in excess of 1.5 *M* would invariably compete with coenzyme binding prior to crystallization within the hanging drop, impeding the formation of a binary or ternary complex. This assertion is validated by our molecular-modelling and mutagenesis results, which showed that the phosphate groups of the modelled $NADP^+$ are in near-identical positions to the sulfate molecules in the crystal structure of DD within the coenzyme-binding domain (Fig. 10) and form a number of similar interactions with residues including Arg37 and Arg41. This suggests that both residues Arg37 and Arg41 are essential to coenzyme binding, somewhat stabilizing the negative charge of the pyrophosphate group. In keeping with our modelling results, we would suggest that the replacement of Ala36, Arg37 and Arg41 by aspartic acid causes the local negative charges to seriously disrupt or repulse the hydrogen-bonding interactions of the phosphate molecules with the arginines, while the mutation of Arg37 and Arg41 to alanine removes any stabilizing interactions that the arginine residues made with the pyrophosphate moieties. Similarly, the hydrophobic pocket created in part by Ala36 for appropriate adenine binding is disrupted by the addition of the charged and more bulky aspartic acid, hence the striking increase in K_d values. This observation more than likely validates our choice of $NADP^+$ model for DD and the positioning of the adenine ring. The importance of these N-terminal arginines and their role in shaping coenzyme stereochemistry is also depicted in our sequence-alignment results (Fig. 5), which show that Arg37 is conserved in TMO but not in GFO and AFR. In addition to the electrostatic interaction with the side chains of Arg37 and Arg41, the stacking interaction of the side chain of Arg37 with the adenine ring may be related to the unique orientation of the adenine-ribose moiety. These interactions may also be responsible for the added affinity (K_m) of NADP(H) for DD (0.56 μ*M*) with respect to the published value for AFR (60 μ*M*; Dambe *et al.*, 2006). Overall, our results demonstrate how the bi-bi mechanism of DD

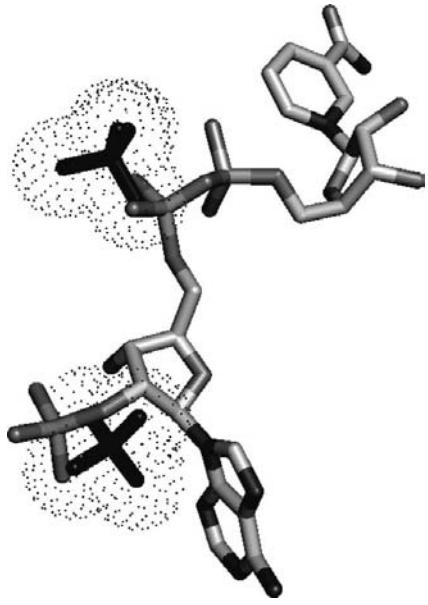

Figure 10
Superimposed of the $NADP^+$ molecule from the modelled DD complex with the sulfate molecules (highlighted with black stippling) present within the coenzyme-binding domain of the DD–IA crystal structure. This figure was prepared using *PyMOL* (DeLano, 2002).

catalysis (Shinoda *et al.*, 1992) and affinity for the coenzyme (Asada *et al.*, 2000; Sato *et al.*, 1993) can be affected by electronegative salts such as sulfate and phosphate, which when present in high enough concentrations ultimately compete with and hinder effective NADP(H) binding, which is primarily stabilized by Arg37 and Arg41.

4.2. Inhibitor-binding site

DD catalyses the oxidoreduction of xenobiotic hydrophobic compounds and sugars and its broader substrate specificity is clearly distinct from those of GFO and AFR, which specifically catabolize hydrophilic sugars (Nurizzo *et al.*, 2001; Kingston *et al.*, 1996; Dambe *et al.*, 2006). The most defining characteristic of the DD–4OH complex when compared with DD–IA is the large number of hydrophobic contacts that it is able to form with residues such as Phe279, Trp254, Leu177 and Leu158. The preference for hydrophobic over any other interaction for effective inhibitor binding in DD was borne out by our active-site mutants, which showed a consistent increase in IC_{50} values when predominantly aliphatic bulky side chains were replaced by residues such as Ala or the polar aromatic Tyr. The K_m (oxidation and reduction) for substrate is also affected, mostly by mutation of Trp125, Trp254 and Phe279. The aliphatic nature of these residues and the ability of DD to catabolize substrates such as aromatic hydrocarbons (Hara, Nakayama *et al.*, 1991; Nakagawa *et al.*, 1989; Sato *et al.*, 1993) are indicative of their important role in the binding of substrate and inhibitor.

4.3. Catalytic mechanism

In the case of the SDR enzymes (Oppermann *et al.*, 2003; Filling *et al.*, 2002; Jornvall *et al.*, 1995; Ishikura *et al.*, 2003; Duax *et al.*, 2000; Tanaka *et al.*, 2001) the catalytic mechanism has been well documented and involves a catalytic triad which forms a proton-relay/hydrogen-transfer system. In these enzymes, tyrosine acts as the catalytic residue responsible for proton transfer, lysine orients the nicotinamide nucleotide moiety of the coenzyme so that it is perpendicular to the reactive substrate and the active-site serine orients the reaction species and forms the active-site consensus sequence Tyr-*X*-*X*-*X*-Lys (Filling *et al.*, 2002; Jornvall *et al.*, 1995). Similarly, the consensus sequence GGX_3DX_3Y first identified by sequence-alignment studies of DD (Arimitsu *et al.*, 1999) has been found to correspond to a loop and active-site α-helix (formed in part by residues 171–180 in DD) which stacks along the C-terminal β-sheet through a series of hydrophobic interactions. The corresponding residues in AFR and GFO also form part of the active site (and the presumed active site of TMO) *via* an α-helical structure that interacts with the C-terminal β-sheet. Like the SDR enzymes, candidate residues within DD identified from the crystal structure together with mutagenesis, modelling and sequence alignment suggest the possibility of a similar mechanism of catalysis in DD that includes residues Tyr180, Lys97 and Asp176. Previous crystal structure analysis has suggested an acid–base catalysis involving residues in similar positions in GFO (Nurizzo *et al.*, 2001) as well as an active-site lysine maintaining coenzyme orientation during catalysis with a definite change in its side chain (with respect to distance from the nicotinamide ring) depending on the oxidation state of the coenzyme and the presence of substrate within the active site. The mutants of Lys97 demonstrate this change in orientation or coenzyme association with respect to oxidation states. K97M and K97R mutants show no activity towards D-xylose and $NADP^+$ and some (however poor) activity in the reduction of CQ and NADPH. Overall size, charge and orientation seem to be important for residues within the vicinity of Lys97, given the preservation of the EKP motif in a large number of enzymes which utilize coenzymes during catalysis (Carbone *et al.*, 2008; Nurizzo *et al.*, 2001; Kingston *et al.*, 1996; Dambe *et al.*, 2006). The formation of a *cis*-peptide by proline helps to maintain the positioning of the lysine adjacent to both the coenzyme and the catalytic residue of DD: Tyr180. Both Lys97 and Tyr180 show exceptionally poor V_{max} values compared with the WT regardless of mutation (Asada *et al.*, 2000), which is indicative of a catalytic residue. Given their proximity, the formation of an intimate catalytic pair or dyad (necessary for acid–base catalysis in the case of the SDR enzymes; Filling *et al.*, 2002; Jornvall *et al.*, 1995; Ishikura *et al.*, 2003; Duax *et al.*, 2000; Tanaka *et al.*, 2001) is more than likely (Fig. 11). Additionally, based on these observations together with the modelled conformation of the nicotinamide ring of the coenzyme, we conclude that DD is most likely to be a *B*-face oxidoreductase.

Adjacent to Tyr180, Asp176, which is conserved in mammalian DD and is similarly present in GFO and AFR (Arimitsu *et al.*, 1999), is more than likely to form a close hydrogen-bond contact that may help to stabilize the substrate, much like the active-site serine in the SDR enzymes, positioning it towards the catalytic tyrosine. This region of the enzyme structure may also indicate a small sugar-binding domain within the predominantly aliphatic active site. Mutagenesis experiments have shown the near-abrogation of activity with respect to the active-site Asp176 and His180 in AFR (Dambe *et al.*, 2006). We would assume that owing to its

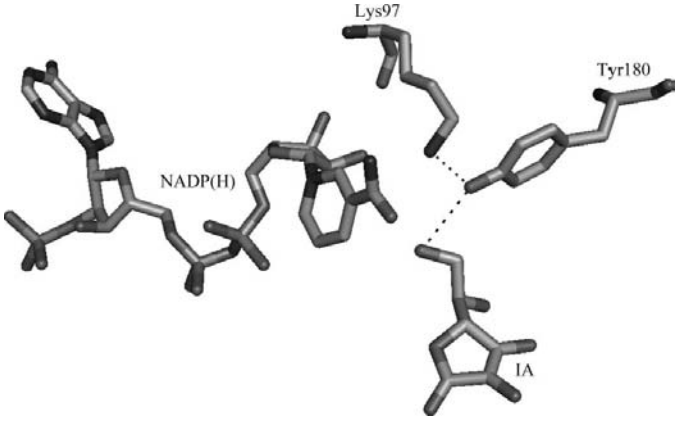

Figure 11
The proposed catalytic dyad of DD: Tyr180 and Lys97 with the inhibitor IA and the modelled $NADP^+$ within the active site of DD following energy minimization. Hydrogen-bonding distances are indicated by dashed lines. This figure was prepared using *PyMOL* (DeLano, 2002).

conserved nature in each sequence Asp176 would form a dynamic part of the active-site domain of DD, GFO and TMO and that His180 in AFR and TMO and Tyr217 in GFO perform the same role as Tyr180 in DD. From these observations, a consensus sequence that would indicate a catalytic similarity and that is found in structurally similar enzymes (at this point), inclusive of both mammalian and bacterial oxidoreductase species, would be GGX_3DX_3(Y/H).

In summary, crystallography, molecular modelling and site-directed mutagenesis were used to identify the intermolecular interactions necessary for coenzyme, substrate and inhibitor binding to mammalian dimeric dihydrodiol dehydrogenase. Ala36, Arg37 and Arg41 are essential for maintaining the proper orientation of the pyrophosphate and adenine-ring moieties of NADP(H), while the characterization of the predominantly hydrophobic active site of DD established that Trp125, Phe154, Trp254 and Phe279 are important residues for the binding of substrate and inhibitor. A mechanism involving the formation of a catalytic dyad (Lys97 and Tyr180) required for the proton-transfer system was also postulated. Crystallization experiment attempts in the absence of salts such as phosphates and sulfates will continue in order to determine the crystal structure of DD in a binary or ternary complex.

We thank Dr Roland Chung for providing the chemical structures of the inhibitors. This work was supported by an Australian Research Council Linkage International Award (to OEK and AH). VC is the recipient of a Monash Centre for Synchrotron Science PhD Scholarship.

References

Aoki, S., Ishikura, S., Asada, Y., Usami, N. & Hara, A. (2001). *Chem. Biol. Interact.* **130–132**, 775–784.

Arimitsu, E., Aoki, S., Ishikura, S., Nakanishi, K., Matsuura, K. & Hara, A. (1999). *Biochem. J.* **342**, 721–728.

Asada, Y., Aoki, S., Ishikura, S., Usami, N. & Hara, A. (2000). *Biochem. Biophys. Res. Commun.* **278**, 333–337.

Bradford, M. M. (1976). *Anal. Biochem.* **72**, 248–254.

Carbone, V., Endo, S., Sumii, R., Chung, R. P.-T., Matsunaga, T., Hara, A. & El-Kabbani, O. (2008). *Proteins*, **70**, 176–187.

Chhabra, S. R., Shockley, K. R., Conners, S. B., Scott, K. L., Wolfinger, R. D. & Kelly, R. M. (2003). *J. Biol. Chem.* **278**, 7540–7552.

Cirilli, M., Zheng, R., Scapin, G. & Blanchard, J. S. (2003). *Biochemistry*, **42**, 10644–10650.

Collaborative Computational Project, Number 4 (1994). *Acta Cryst.* D**50**, 760–763.

Dambe, T. R., Kuhn, A. M., Brossette, T., Giffhorn, F. & Scheidig, A. J. (2006). *Biochemistry*, **45**, 10030–10042.

Darmanin, C. & El-Kabbani, O. (2000). *Bioorg. Med. Chem. Lett.* **10**, 1101–1104.

Darmanin, C. & El-Kabbani, O. (2001). *Bioorg. Med. Chem. Lett.* **11**, 3133–3136.

DeLano, W. L. (2002). *The PyMOL Molecular Graphics System.* DeLano Scientific, San Carlos, USA.

Deyashiki, Y., Ohshima, K., Nakanishi, M., Sato, K., Matsuura, K. & Hara, A. (1995). *J. Biol. Chem.* **270**, 10461–10467.

Duax, W. L., Ghosh, D. & Pletnev, V. (2000). *Vitam. Horm.* **58**, 121–148.

Emsley, P. & Cowtan, K. (2004). *Acta Cryst.* D**60**, 2126–2132.

Filling, C., Berndt, K. D., Benach, J., Knapp, S., Prozorovski, T., Nordling, E., Ladenstein, R., Jornvall, H. & Oppermann, U. (2002). *J. Biol. Chem.* **277**, 25677–25684.

Hara, A., Matsuura, K., Tamada, Y., Sato, K., Miyabe, Y., Deyashiki, Y. & Ishida, N. (1996). *Biochem. J.* **313**, 373–376.

Hara, A., Nakayama, T., Harada, T., Kanazu, T., Shinoda, M., Deyashiki, Y. & Sawada, H. (1991). *Biochem. J.* **275**, 113–119.

Hara, A., Shinoda, M., Kanazu, T., Nakayama, T., Deyashiki, Y. & Sawada, H. (1991). *Biochem. J.* **275**, 121–126.

Hyndman, D., Bauman, D. R., Heredia, V. V. & Penning, T. M. (2003). *Chem. Biol. Interact.* **143–144**, 621–631.

Ishikura, S., Isaji, T., Usami, N., Nakagawa, J., El-Kabbani, O. & Hara, A. (2003). *Chem. Biol. Interact.* **143–144**, 543–550.

Jornvall, H., Danielsson, O., Hjelmqvist, L., Persson, B. & Shafqat, J. (1995). *Adv. Exp. Med. Biol.* **372**, 281–294.

Kingston, R. L., Scopes, R. K. & Baker, E. N. (1996). *Structure*, **4**, 1413–1428.

Kraulis, P. J. (1991). *J. Appl. Cryst.* **24**, 946–950.

Krissinel, E. & Henrick, K. (2004). *Acta Cryst.* D**60**, 2256–2268.

Luzzati, V. (1952). *Acta Cryst.* **5**, 802–810.

McPherson, A. (1985). *Methods Enzymol.* **114**, 112–120.

Matthews, B. W. (1968). *J. Mol. Biol.* **33**, 491–497.

Murshudov, G. N., Vagin, A. A. & Dodson, E. J. (1997). *Acta Cryst.* D**53**, 240–255.

Nakagawa, M., Matsuura, K., Hara, A., Sawada, H., Bunai, Y. & Ohya, I. (1989). *J. Biochem. (Tokyo)*, **106**, 1104–1109.

Nakayama, T., Sawada, H., Deyashiki, Y., Kanazu, T., Hara, A., Shinoda, M., Matsuura, K., Bunai, Y. & Ohya, I. (1990). *Adv. Exp. Med. Biol.* **284**, 187–196.

Nurizzo, D., Halbig, D., Sprenger, G. A. & Baker, E. N. (2001). *Biochemistry*, **40**, 13857–13867.

Oppermann, U., Filling, C., Hult, M., Shafqat, N., Wu, X., Lindh, M., Shafqat, J., Nordling, E., Kallberg, Y., Persson, B. & Jornvall, H. (2003). *Chem. Biol. Interact.* **143–144**, 247–253.

Otwinowski, Z. & Minor, W. (1997). *Methods Enzymol.* **276**, 307–326.

Penning, T. M. (2004). *Methods Enzymol.* **378**, 31–67.

Sato, K., Inazu, A., Yamaguchi, S., Nakayama, T., Deyashiki, Y., Sawada, H. & Hara, A. (1993). *Arch. Biochem. Biophys.* **307**, 286–294.

Sato, K., Nakanishi, M., Deyashiki, Y., Hara, A., Matsuura, K. & Ohya, I. (1994). *J. Biochem. (Tokyo)*, **116**, 711–717.

Shinoda, M., Hara, A., Nakayama, T., Deyashiki, Y. & Yamaguchi, S. (1992). *J. Biochem. (Tokyo)*, **112**, 840–844.

Tanaka, N., Nonaka, T., Nakamura, T. K. & Hara, A. (2001). *Curr. Org. Chem.* **5**, 89–111.

Thompson, J. D., Gibson, T. J., Plewniak, F., Jeanmougin, F. & Higgins, D. G. (1997). *Nucleic Acids Res.* **25**, 4876–4882.

Wörner, W. & Oesch, F. (1984). *FEBS Lett.* **170**, 263–267.

Zepeda, S., Monasterio, O. & Ureta, T. (1990). *Biochem. J.* **266**, 637–644.